https://doi.org/10.15407/ujpe70.5.315

V.O. KHARCHENKO,[1,2] D.O. KHARCHENKO,[1] A.V. DVORNICHENKO,[2] B.O. LYSENKO,[1] S.V. KOKHAN[1]

[1] Institute of Applied Physics, Nat. Acad. of Sci. of Ukraine
(58, Petropavlivs'ka Str., Sumy 40000, Ukraine; e-mail: vasiliy@ipfcentr.sumy.ua)

[2] Sumy State University
(116, Kharkivsk'a Str., Sumy 40000, Ukraine)

SIMULATION OF MICROSTRUCTURAL TRANSFORMATIONS IN Fe–Cr–Al ALLOYS UNDER NEUTRON IRRADIATION

Theoretical studies of the influence of irradiation conditions on the microstructure evolution in Fe–Cr–Al alloys and the statistical properties of α'-phase precipitates have been carried out. In the framework of the stability analysis, phase diagrams that describe the range of parameters for the implementation of the precipitation processes during thermal annealing and irradiation are determined. Numerical simulation is applied to study the influence of the irradiation on the kinetics of precipitates and the changes in their statistical characteristics. It is shown that the temperature growth at the irradiation leads to the same effects as a damage rate reduction owing to the competition between the ballistic mixing, which is responsible for the instability of homogeneous configuration, and the thermodynamic force that suppresses such an instability.

Keywords: phase separation, secondary phase precipitates, neutron irradiation, numerical simulation.

1. Introduction

During the last five decades, Fe–Cr–Al alloys have attracted attention in various fields of application, including their use in nuclear power engineering. A number of various Fe–Cr–Al alloys with different chromium (Cr) and aluminum (Al) contents have been developed and subjected to comprehensive evaluation. These evaluations covered aspects such as fuel cladding compatibility, high temperature effects, aging, radiation effects, and other parameters [1].

Citation: Kharchenko V.O., Kharchenko D.O., Dvornichenko A.V., Lysenko B.O., Kokhan S.V. Simulation of microstructural transformations in Fe–Cr–Al alloys under neutron irradiation. *Ukr. J. Phys.* **70**, No. 5, 315 (2025). https:// doi.org/10.15407/ujpe70.5.315.

© Publisher PH "Akademperiodyka" of the NAS of Ukraine, 2025. This is an open access article under the CC BY-NC-ND license (https://creativecommons.org/licenses/by-nc-nd/4.0/)

A detailed analysis of the properties of those alloys has shown that the addition of Cr and Al is a crucial factor for improving the oxidation resistance of the alloys at high temperatures [2–4]. This goal is achieved by creating continuous protective layers of aluminum oxide on the material surface [5, 6]. A control over the physical and mechanical properties of these alloys requires that the percentage composition of the alloy – in particular, the Cr and Al contents – has to be balanced. This balance helps one to prevent the formation of brittle phases such as σ-FeCr or α'-Cr. The formation of the α'-phase in Fe–Cr–Al alloys used as fuel cladding, for example, in light water reactors (at temperatures below 500 °C) can induce substantial hardening and embrittlement of the alloy [7]. The mentioned embrittlement mechanism has prompted efforts to develop alloys that preserve the oxidation resistance of Fe–Cr–Al alloys with a high Al content

(>18 wt%) – e.g., Kanthal APMT, PM2000, *etc.* – but with a much lower Cr content. The reduced Cr content is compensated by increasing the Al concentration. Previous studies of radiation effects showed that Fe–Cr–Al alloys have a behavior similar to that of other Cr-rich ferritic alloys, whereas the addition of Al can induce changes in certain alloy properties [8].

The studies of model Fe–Cr–Al alloys subjected to the neutron irradiation are mostly associated with radiation hardening caused by α'-precipitates and dislocation loops that grow during the irradiation. The precipitation of α'-precipitates in the course of the irradiation is mostly related to the radiation-accelerated diffusion of atoms owing to their ballistic mixing. It was experimentally demonstrated that the size of precipitates and their concentration depend not only on the content of alloying Cr and Al, but also on irradiation conditions (the damage rate and the temperature) [9–12]. It was shown that the typical size of these precipitates under the neutron irradiation is about $2-4$ nm with a corresponding concentration of about $(2\div3)\times10^{24}$ m^{-3}.

Together with experimental studies of the microstructure and the physical and mechanical properties of Fe–Cr–Al alloys, various theoretical and numerical modeling methods are widely used to study the precipitation kinetics. The results of first-principles calculations, molecular dynamics simulations, and Monte Carlo simulations presented in work [13] showed that the main source of complexity of such systems is the non-monotonic dependences of a large number of quantities and properties that characterize their thermodynamic behavior on the Cr concentration. In works [14–17], a comprehensive strategy was proposed to study the kinetics of the nanoscale α'-phase. This strategy combines various techniques, including first-principles calculations, CALPHAD simulations, and experimental studies. The CALPHAD approach, which is based on the Gibbs energy [18], has proved its highly efficiency when determining phase diagrams for equilibrium thermodynamic conditions. It is a valuable tool for component selection, composition design, and material optimization for specific applications.

Recent progress in this domain has improved the understanding of microstructural changes in Fe–Cr–Al systems. However, open questions still exist concerning the microstructure evolution under the influence of neutron irradiation. A comprehensive study of the α'-phase stability and precipitation processes under irradiation should consider the evolution of the defect structure and the effects of ballistic mixing of the atoms induced by the irradiation [19–31]. Such processes affect the local rearrangement of the atoms of alloying elements as a result of the irradiation-enhanced diffusion.

In this work, attention is focused on the analysis of how the irradiation temperature and the damage rate affect the microstructure evolution in Fe–Cr–Al alloys and on the statistical properties of α'-phase precipitates under constant irradiation conditions. Our approach is based on the application of the phase field approach in combination with the CALPHAD method [18] and the theory of reaction rates for non-equilibrium point defects [32], with regard for the effects of ballistic mixing of atoms [19, 23]. Such a combined approach allows a detailed analysis of the alloy microstructure evolution to be carried out, the stability of α'-phase precipitates under the action of radiation to be analyzed, and the influence of irradiation conditions on statistical alloy characteristics to be found. In addition, this approach makes it possible to study the local reorganization of point defects in irradiated alloys.

The paper is organized as follows. In the next section, a mathematical model is constructed for Fe–Cr–Al systems. The main results of the work are presented in Section 3. In particular, in Section 3.1, phase diagrams that determine the stability parameters of the α'-phase precipitates are obtained in the framework of the stability analysis. The dynamics of the changes in the alloy microstructure and the statistical characteristics of precipitates during the irradiation under various conditions is studied in Section 3.2 using numerical simulation methods. Main conclusions of the work are drawn in Section 4.

2. Model

When considering the ternary alloy Fe–Cr–Al, we deal with atomic and defect subsystems and operate with atomic (molar) concentrations of elements and the corresponding concentration of point defects. The atomic subsystem is described by the molar concentrations of the alloy components in the standard way: $x_\mu = N_\mu/N$, where N_μ determines the number of atoms of the μ-type ($\mu = \{\mathrm{Fe}, \mathrm{Cr}, \mathrm{Al}\}$), and N is the total number of atoms. For the atomic subsystem, we

use the law of mass conservation $\sum_\mu x_\mu = 1$ and consider a system with a constant volume. To describe the system of point defects, we denote their concentration as $c_d = N_d/N$, where N_d is the number of corresponding defects of the d-type ($d = \{i, v\}$, where i/v means interstitials/vacancies).

The total Gibbs energy functional for the system under consideration has the standard form

$$\mathcal{G} = \frac{1}{V_m}\int_V [G_{\mathrm{Fe-Cr-Al}}(\{x_\mu\}) + G_d(\{c_d\}) + \\ + G_\nabla(\{\nabla x_\mu\}, \{\nabla c_d\})]\,\mathrm{d}\mathbf{r}, \quad (1)$$

where V_m is the molar volume. The molar Gibbs energy of the atomic subsystem, $G_{\mathrm{Fe-Cr-Al}}$, is determined using the CALPHAD method:

$$G_{\mathrm{Fe-Cr-Al}} = G^{\mathrm{ref}}_{\mathrm{Fe-Cr-Al}} + G^{\mathrm{id}}_{\mathrm{Fe-Cr-Al}} + G^{\mathrm{ex}}_{\mathrm{Fe-Cr-Al}}.$$

Here, $G^{\mathrm{ref}}_{\mathrm{Fe-Cr-Al}} = \sum_\mu G^0_\mu x_\mu$ is the Gibbs energy, which is determined by the potentials G^0_μ from the SGTE (Scientific Group Thermodata Europe) database [18]. The term

$$G^{\mathrm{id}}_{\mathrm{Fe-Cr-Al}} = RT\sum_\mu x_\mu \ln x_\mu,$$

where R is the universal gas constant, and T is the temperature, describes the entropy contribution associated with the random mixing of atoms. Finally, the tern $G^{\mathrm{ex}}_{\mathrm{Fe-Cr-Al}} = \sum_{\mu\neq\nu} x_\mu x_\nu L_{\mu,\nu}$ is determined by the temperature-dependent interaction coefficients $L_{\mu,\nu}$.

The Gibbs energy G_d for the subsystem of point defects $d = \{i, v\}$ can be written in the form $G_d = \sum_{d=i,v} G^f_d + G^{\mathrm{id}}_d + G^{\mathrm{int}}_d$. The formation energy G^f_d of the corresponding defect in the alloy is determined via the defect formation energies in pure materials, $G^{f,\mu}_d$, and the nominal atomic concentrations in the alloy x^0_μ: $G^f_d = \sum_\mu x^0_\mu G^{f,\mu}_d$. The corresponding entropic contribution has the form $G^{\mathrm{id}}_d = RTc_d \ln c_d$. The interaction energies between defects and atoms G^{int}_d are defined as $G^{\mathrm{int}}_d = c_d \sum_\mu x^0_\mu G^{\mathrm{int}}_{d-\mu}$, where, for the defect-atom interaction energies, we use the following definition [33]: $G^{\mathrm{int}}_{d-\mu} = (G^\mu_{\mathrm{coh}} + G^{f,\mu}_d)/Z$, where G^μ_{coh} is the cohesion energy, and Z is the coordination number.

The gradient term G_∇ in Eq. (1) looks like

$$G_\nabla = \sum_\mu \frac{\kappa_\mu}{2}(\nabla x_\mu)^2 + \sum_d \frac{\kappa_d}{2}(\nabla c_d)^2, \quad (2)$$

where, according to the Hilliard approach [34], $\kappa_{\mathrm{Fe}} = \kappa_{\mathrm{Cr}} = \kappa_{\mathrm{Al}} = \kappa$ and $\kappa = L_{\mathrm{Fe,Cr}} a_0^2/6$, $a_0 = \sum_\mu a^\mu_0 x^0_\mu$ is the effective lattice constant, and a^μ_0 are the lattice constants for pure elements. For the constants $\kappa_i = \kappa_v$, let us use the formalism considered in works [35, 36] and fix their values to be 6.91×10^{-9} J/m.

In view of the effects of ballistic mixing of atoms induced by the action of irradiating sources [23, 37], the dynamics of the atomic subsystem is described by the following equation:

$$\partial_t x_\mu = \nabla \cdot \sum_\nu M_{\mu,\nu} \nabla \frac{\delta \mathcal{G}}{\delta x_\nu} + \Gamma(\langle x_\mu \rangle_w - x_\mu). \quad (3)$$

The kinetic coefficients $M_{\mu,\nu}$ are determined in a standard way [38, 39]:

$$\begin{aligned} &M_{\mathrm{Cr,Cr}} = x_{\mathrm{Cr}}\left[(1-x_{\mathrm{Cr}})^2 M_{\mathrm{Cr}} + \right. \\ &\left. + x_{\mathrm{Cr}} x_{\mathrm{Al}} M_{\mathrm{Al}} + x_{\mathrm{Cr}} x_{\mathrm{Fe}} M_{\mathrm{Fe}}\right], \\ &M_{\mathrm{Al,Al}} = x_{\mathrm{Al}}\left[(1-x_{\mathrm{Al}})^2 M_{\mathrm{Al}} + \right. \\ &\left. + x_{\mathrm{Al}} x_{\mathrm{Fe}} M_{\mathrm{Fe}} + x_{\mathrm{Al}} x_{\mathrm{Cr}} M_{\mathrm{Cr}}\right], \\ &M_{\mathrm{Cr,Al}} = x_{\mathrm{Cr}} x_{\mathrm{Al}}\left[x_{\mathrm{Fe}} M_{\mathrm{Fe}} - \right. \\ &\left. - (1-x_{\mathrm{Cr}}) M_{\mathrm{Cr}} - (1-x_{\mathrm{Al}}) M_{\mathrm{Al}}\right]. \end{aligned} \quad (4)$$

Here M_μ are the corresponding mobilities for pure elements, which are determined in the standard way: $M_\mu = D_\mu/RT$, where D_μ is the diffusion coefficient of μ-th atoms. The last term in Eq. (3) describes the ballistic mixing of atoms caused by the irradiation, where the averaging is performed over the probability distribution $w(\mathbf{r})$ [23, 37],

$$\langle x_\mu \rangle_w \equiv \int w(\mathbf{r}-\mathbf{r}') x_\mu(\mathbf{r}')\mathrm{d}\mathbf{r}',$$

where $w(r) = e^{-r/d_r}/(2\pi d^2)$ [37], and d is the average displacement distance [37]. The atomic jump frequency is $\Gamma = \mathcal{K}A$, where $\mathcal{K}$ is the dose rate calculated according to the NRT standard [40], and $A = 50$ for the neutron irradiation [41]. The accumulated radiation dose equals $\phi = \mathcal{K}t$.

With regard for the law of mass conservation and defining the iron concentration as the main one, $x_{\mathrm{Fe}} = 1 - x_{\mathrm{Cr}} - x_{\mathrm{Al}}$, the evolution of the atomic subsystem is given by two equations of type (3) for the chromium and aluminum concentrations.

The evolution equation for non-equilibrium point defects has the form

$$\partial_t c_d = \nabla \cdot L_d \nabla \frac{\delta \mathcal{G}}{\delta c_d} + \mathcal{K} - D_d k_d^2 c_d - \alpha_r c_i c_v. \quad (5)$$

Model parameters

Parameter	Dimension	Value	Reference
a_{Fe}, a_{Cr}, a_{Al}	nm	0.286, 0.291, 0.405	
G^0_{Fe}	J/mol	$1225.7 + 124.134T - 23.5143T\ln(T) - $ $- 0.439752 \times 10^{-2}T^2 - 0.589269 \times 10^{-7}T^3 + \frac{77358.5}{T}$	[18]
G^0_{Cr}	J/mol	$-8856.94 + 157.48T - 26.908T\ln(T) + $ $+ 0.189435 \times 10^{-2}T^2 - 0.147721 \times 10^{-5}T^3 + \frac{139250}{T}$	[18]
G^0_{Al}	J/mol	$-1193.24 + 218.235446T - 38.5844296T\ln(T) + $ $+ 0.018531982T^2 - 0.576227 \times 10^{-5}T^3 + \frac{74092}{T}$	[18]
$L_{\mathrm{Fe,\,Cr}}$	J/mol	$20500 - 9.68T$	[18]
$L_{\mathrm{Cr,\,Al}}$	J/mol	$-54900 + 10T$	[18]
$L_{\mathrm{Fe,\,Al}}$	J/mol	$-122452.9 + 31.6455T$	[18]
$E^f_{i,\,\mathrm{Fe}}$	eV	3.52	[42]
$E^f_{v,\,\mathrm{Fe}}$	eV	1.4	[43]
$G^{\mathrm{coh}}_{\mathrm{Fe}}$	J/mol	413000	[44]
$E^f_{i,\,\mathrm{Cr}}$	eV	3.356	[45]
$E^f_{v,\,\mathrm{Cr}}$	eV	1.36	[46]
$G^{\mathrm{coh}}_{\mathrm{Cr}}$	J/mol	395000	[44]
D_{Fe}	m^2/s	$2.8 \times 10^{-4}\exp(-251000/RT)$	[16]
D_{Cr}	m^2/s	$3.7 \times 10^{-3}\exp(-267000/RT)$	[16]
D_{Al}	m^2/s	$5.2 \times 10^{-4}\exp(-246000/RT)$	[16]
D_v	m^2/s	$3.84 \times 10^{-4}\exp(-300000/RT)$	[35]
D_i	m^2/s	$2.05 \times 10^{-4}\exp(-280000/RT)$	[35]
ρ_N	m^2/s	10^{14}	[47]

Here, the first summand describes the corresponding diffusion flux with the mobility $L_d = D_d c_d/(RT)$ that is determined via the corresponding point-defect diffusion coefficient D_d, k_d is the absorption rate of vacancies and interstitial atoms by sinks (dislocations, loops, grain boundaries, *etc.*), and the defect recombination rate $\alpha_r \approx 4\pi r_{iv} D_i/\Omega_0$ is determined by the defect recombination radius r_{iv} and the atomic volume Ω_0 [33]. To simplify the description of the dynamics of point defects playing the role of sinks for vacancies and interstitial atoms, let us consider only the dislocation network density ρ_N: $k_d^2 = Z_N^d \rho_N$, where $Z_N^d \approx \frac{\ln(1/\rho_N^{1/2} r_0)}{\ln(2/\rho_N^{1/2} r_0) - \gamma}$, $r_0 = 2b$, b is the magnitude of the Burgers vector, and γ is the Euler constant [32].

3. Results

When carrying out theoretical studies of the influence of irradiation conditions on the microstructure evolution and the change in the statistical properties of precipitates of the α'-phase, it is necessary, first of all, to simulate of the precipitation of precipitates in the alloy at its heat treatment. The obtained microstructure will be used as a target for modeling the influence of the irradiation. The main model parameters are quoted in Table. For the further research, it is convenient to use a dimensionless system by introducing the dimensionless time t'^2/D_{Al} and the dimensionless distance $\mathbf{r}' = \mathbf{r}/\ell$, where $\ell = a_0$. For the average distance of ballistic displacements, we put $d = a_0$.

3.1. Stability diagrams

In order to determine the values of main parameters – they are reduced to the irradiation temperature T and the damage intensity $\mathcal{K}$ – if the precipitation of chromium precipitates becomes possible, let us analyze the stability of homogeneous stationary states with respect to inhomogeneous perturbations. At this

stage, we neglect the contribution of the defect subsystem and analyze the atomic system described by Eqs. (3). For this purpose, let us consider the perturbation $\delta x_\mu = x_\mu - x_\mu^0$ and seek the corresponding solution in the form $\delta x_\mu \propto \exp(\lambda t + ikr)$. Substituting it into Eqs. (3), we obtain the dependence of the stability index λ on the wave number k. An analysis of the obtained dependences $\lambda(k)$ makes it possible to determine conditions for the phase separation processes to take place. In the case $\lambda_{1,2}(k) < 0$, the system becomes homogenized for all k (solid solution implementation). In the case $\lambda_1(k) > 0$ or $\lambda_2(k) > 0$ at $k \in (0, k_c)$, phase separation processes will occur in the course of system evolution.

By changing the chromium concentration and the annealing temperature, we obtained a phase diagram for alloys with various aluminum concentrations, which is shown in Fig. 1. Here, the dashed curves correspond to heat treatment processes ($\mathcal{K} = 0$), and the solid curves correspond to irradiated systems with the damage rate $\mathcal{K} = 10^{-6}$ displacement per atom per second (dpa/s). Typical dependences of the stability index in the phase separation region and in the solid solution region are plotted in Fig. 2.

From Fig. 1, we can see that the growth of the aluminum concentration expands the interval of chromium concentration values at which the precipitation of α'-phase precipitates is possible (inside the bounded region). In addition, aluminum induces phase separation processes at elevated temperatures, which are realized under conditions of increased chromium concentrations in Fe–Cr–Al alloys. The ballistic mixing of atoms induced by irradiation gives rise to a reduction of the region where the precipitation processes of α'-phase precipitates can be realized at low temperatures. Here, the ballistic flux brings about a structural disorder and, as a result, the dissolution of possibly existing precipitates in the annealed alloy at low temperatures.

In order to analyze in detail the influence of the competition between the thermal and ballistic fluxes on microstructural changes in Fe–Cr–Al alloys under irradiation, let us consider the diagram $\mathcal{K}(T)$ presented in Fig. 3. The phase separation region is limited by the maximum value $\mathcal{K}_c$ of the defect formation rate, as well as the minimum, T_{c1}, and maximum, T_{c2}, values of irradiation temperature. One can see that an increase in the damage rate at a fixed irradiation temperature (or a temperature decrease at a fixed-dose rate) brings about the alloy homogenization. In such cases, a decisive role in the processes of microstructural transformations is played by ballistic mixing ef-

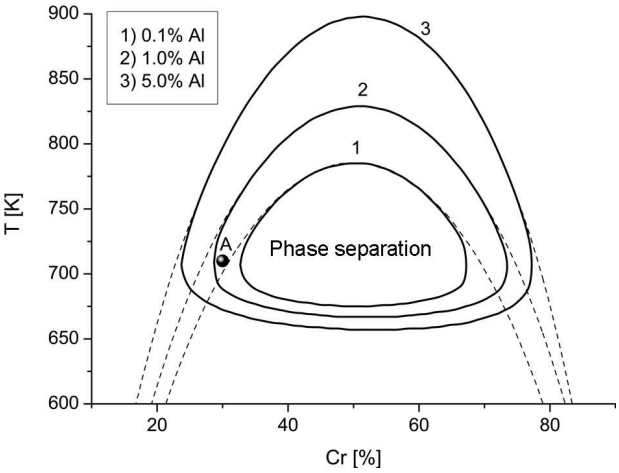

Fig. 1. Phase diagrams for Fe–Cr–Al alloys with various aluminum contents. Dashed curves correspond to non-irradiated systems. Solid curves correspond to irradiated systems at $\mathcal{K} = 10^{-6}$ dpa/s

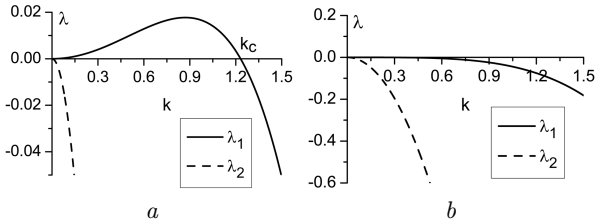

Fig. 2. Typical dependences $\lambda(k)$ for the stability index: in the phase separation region (a), in the solid-solution region. See further explanations in the text (b)

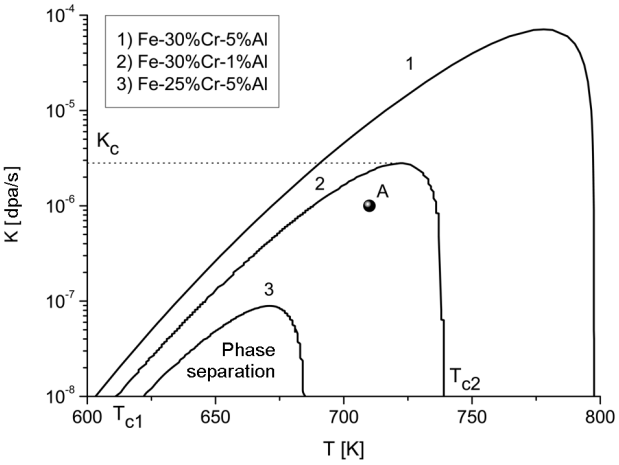

Fig. 3. Phase diagrams for various Fe–Cr–Al alloys

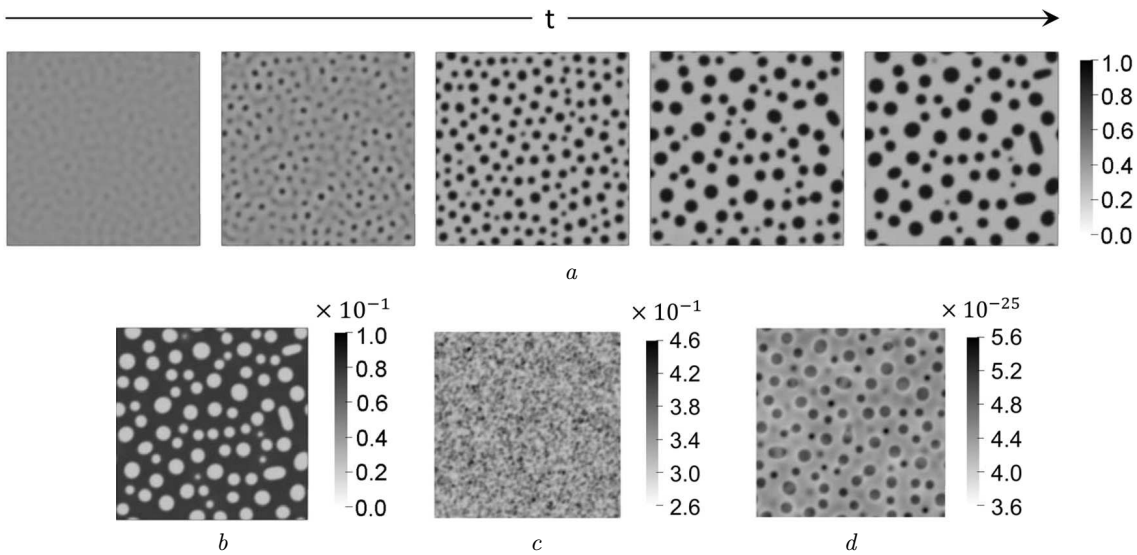

Fig. 4. Evolution of the chromium concentration field in the Fe-30%Cr-5%Al alloy (a). Distributions of aluminum concentration (b), vacancy concentration (c), and interstitial concentration in the annealed specimen (d)

fects. By comparing the obtained dependences $\mathcal{K}(T)$ for alloys with various concentrations of alloying elements, we find that the reduction of both chromium and aluminum concentrations diminishes the maximum value of the damage rate $\mathcal{K}_c$ and narrows the temperature interval, where the precipitation of α'-phase precipitates becomes possible.

3.2. Numerical simulation

To analyze the precipitation dynamics for α'-phase precipitates, we numerically solved Eqs. (3)–(5) on a two-dimensional $N \times N$ "cubic" lattice ($N = 128$) of linear size $L = N\Delta x$ with periodic boundary conditions. Integration over coordinates was performed with the dimensionless step $\Delta x' = 1$ using the Fourier spectral method [48–50]. Integration over the time t' was performed with the step $(\Delta t')^{-3}$.

First, a target should be formed: an annealed alloy with a predetermined microstructure. On the basis of the stability analysis, we took the Fe-30%Cr-5%Al alloy as a model system. It was subjected to the heat treatment at the temperature $T = 710$ K (point A in Figs. 1 and 3). We chose the following initial configurations for the concentrations of alloying elements and point defects: $\langle x_\mu(0)\rangle = x_\mu^0$, $\langle c_d(0)\rangle = c_d^{eq}$; $\langle (x_\mu(0) - x_\mu^0)^2\rangle = 10^{-3}x_\mu^0$, and $\langle (c_d(0) - c_d^{eq})^2\rangle = 10^{-3}c_d^{eq}$, where c_d^{eq} is the equilibrium concentration of point defects.

A typical scenario of phase decay during the heat treatment of the Fe-30%Cr-5%Al solid solution is illustrated in Fig. 4, a. Here, the spatial distribution of the local chromium concentration is shown by the gray scale: from 0 (white) to 1 (black). One can see that, as was discussed in work [17], after a certain critical time interval t_c depending on the heat treatment conditions and alloy composition, the interaction and thermal diffusion processes lead to the formation of a large number of chromium-enriched domains. These domains grow in size and, if annealing continues, their number decreases because small precipitates (whose size is smaller than the critical one) dissolve. In this case, the large precipitates accumulate material from the matrix and continue to grow according to the Ostwald scenario.

Panels b to d in Fig. 4 demonstrate the distributions of local concentrations of aluminum, equilibrium vacancies, and equilibrium interstitial atoms in the annealed specimen. One can see that aluminum becomes uniformly dissolved in the iron matrix. Equilibrium vacancies are quasi-homogeneously distributed over the alloy, whereas interstitial atoms are mainly concentrated in small precipitates and in large ones near the interface.

The obtained concentration distributions of the alloying elements and point defects were chosen as an annealed alloy target to study the influence of the irradiation temperature T and the defect generation

rate $\mathcal{K}$ on the microstructure evolution and the statistical characteristics of the available precipitates of the α'-phase. The evolution of the chromium and aluminum concentration fields in the Fe-30%Cr-5%Al alloy under irradiation at the dose rate $\mathcal{K} = 10^{-6}$ dpa/s is exhibited in Fig. 5.

One can see that, with the accumulation of the irradiation dose ϕ, the average size of precipitates increases, whereas their number decreases. This effect is associated with the accelerated absorption of dissolved chromium atoms from the matrix by the existing precipitates. At the same time, the distribution of aluminum in the alloy remains uniform over the iron matrix.

A typical evolution of the spatial distributions of non-equilibrium vacancies and interstitial atoms in the Fe-30%Cr-5%Al alloy in the course of neutron irradiation is shown in Fig. 6. It can be seen that, with the accumulation of irradiation dose, vacancies are concentrated mostly at the phase interface, whereas interstitial atoms are mostly concentrated in chromium precipitates.

Now, let us focus attention on studying the influence of the irradiation temperature and the damage rate on the dynamics and statistical properties of precipitates of the α'-phase. As the main statistical characteristics, we considered the number of precipitates N_p, their average linear size $\langle R_p \rangle = N_p^{-1} \sum R_p$, and the size distribution of precipitates $f(R^*)$, where $R^* = R_p/\langle R_p \rangle$. To identify the presence of precipitates, we used the chromium concentration threshold $x^c_{\mathrm{Cr}} = 0.5$ under the condition $x_{\mathrm{Cr}}(\mathbf{r}) > x^c_{\mathrm{Cr}}$. The linear size of precipitates R_p was associated with the radius of a circle with identical area. In this case, the obtained dimensionless value of the precipitate radii R'_p measured in $\Delta x'$ units can be converted into dimensional units using the relationship $R_p = R'_p \ell$. To calculate the radii and the number of precipitates, we used the percolating cluster approach with regard for the periodic boundary conditions. The dependences of the average size of precipitates, $\langle R_p \rangle$, and the number of precipitates, N_p, on the irradiation dose ϕ for the annealed Fe-30%Cr-5%Al alloy under various irradiation conditions are depicted in Figs. 7 and 8, respectively. It is evident that the character of the evolution of each parameter does not depend on irradiation conditions.

From the obtained results, it follows that, in the annealed alloy, there were approximately 80 precipitates with an average size of about 2.8 nm. Let us firstly consider the case of irradiation corresponding to $\mathcal{K} = 10^{-6}$ dpa/s and $T = 710$ K described by solid curves in Figs. 7 and 8. we can see that, at irradiation to a dose of $\phi \sim 10^{-2}$ dpa, neither the number of precipitates nor their average size changes considerably. As the irradiation dose increases, the number of precipitates gradually decreases, whereas their average size increases. After this transient regime accompanied by a further radiation dose accumulation, a certain universal dynamics is observed for both examined quantities, namely, $\langle R_p \rangle(\phi) \propto \phi^a$ and $N_p(\phi) \propto \exp(-t/t_c)$, where the parameters a and t_c depend on the irradiation conditions.

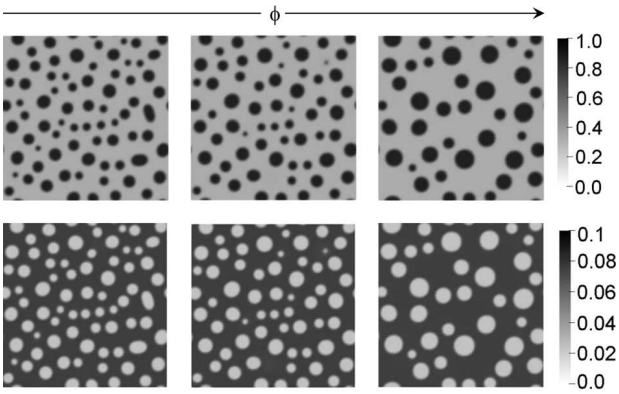

Fig. 5. Evolution of the chromium (upper panels) and aluminum (lower panels) concentration fields in the Fe-30%Cr-5%Al alloy under irradiation at the dose rate $\mathcal{K} = 10^{-6}$ dpa/s and the temperature $T = 710$ K

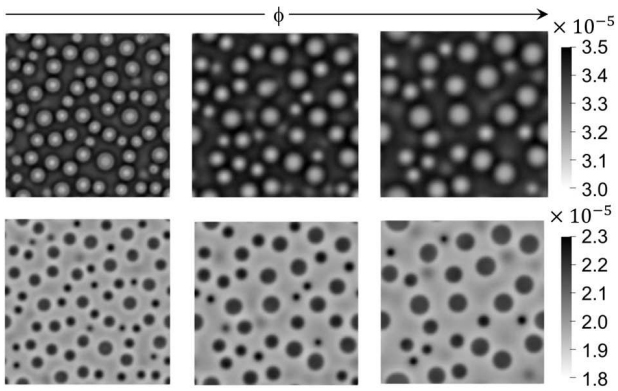

Fig. 6. Typical evolution of the spatial distributions of non-equilibrium vacancies (upper panels) and interstitial atoms (lower panels) in the Fe-30%Cr-5%Al alloy under irradiation at the dose rate $\mathcal{K} = 10^{-6}$ dpa/s and the temperature $T = 710$ K

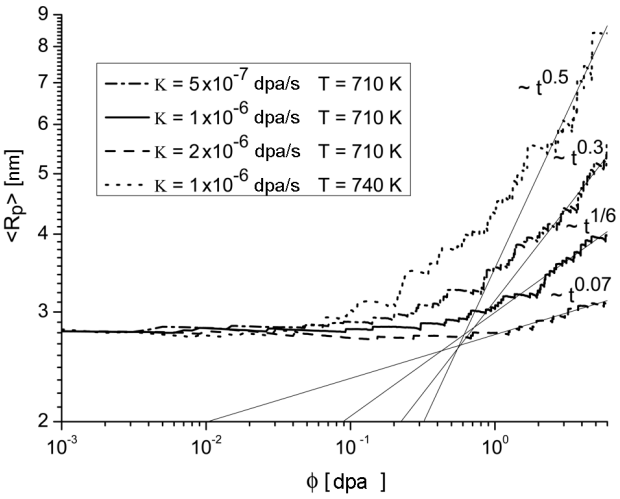

Fig. 7. Dependence of the average precipitate size $\langle R_p \rangle$ on the irradiation dose ϕ for the annealed alloy Fe-30%Cr-5%Al under various irradiation conditions

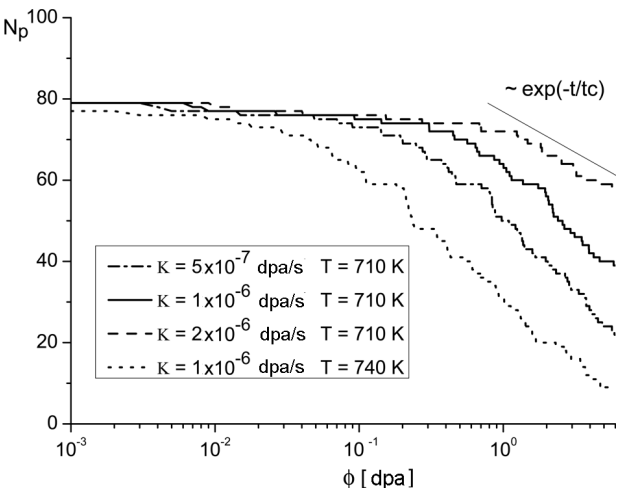

Fig. 8. Dependence of the precipitate number N_p on the irradiation dose ϕ for the annealed Fe-30%Cr-5%Al alloy under various irradiation conditions

The growth of the irradiation temperature to 740 K accelerates the processes of microstructural changes as a result of the thermal diffusion enhancement (cf. the solid and dashed curves in Figs. 7 and 8). A similar effect is observed when the dose rate is reduced to 5×10^{-7} dpa/s (cf. the solid and dashed-dotted curves in Figs. 7 and 8). On the contrary, an increase in the dose rate to 2×10^{-6} dpa/s slows down the processes of precipitate interaction, which is a result of the dominant ballistic diffusion (cf. the solid

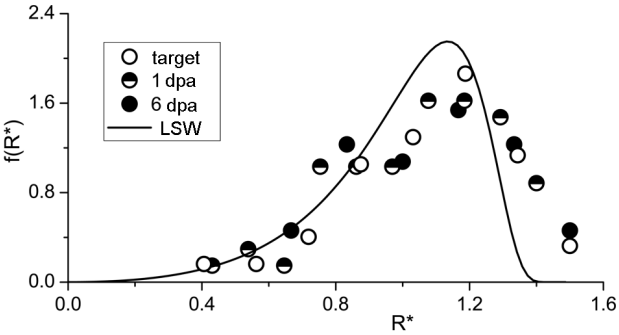

Fig. 9. Precipitate size distributions $f(R^*)$ for the annealed alloy Fe-30%Cr-5%Al irradiated to various irradiation doses ϕ at $T = 710$ K and $\mathcal{K} = 10^{-6}$ dpa/s

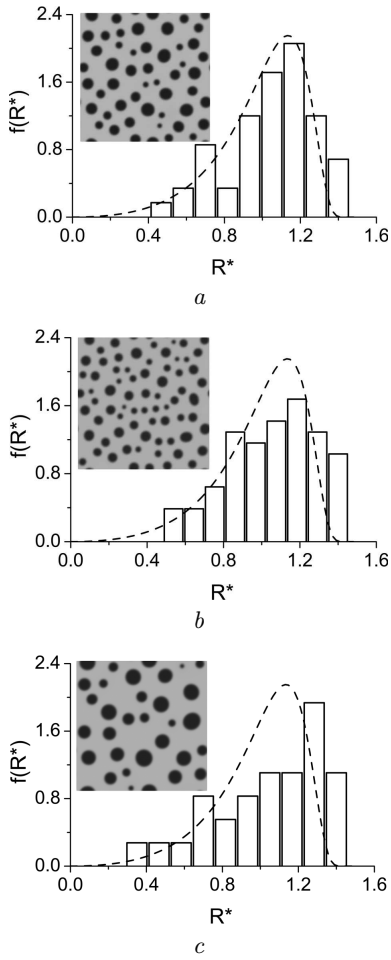

Fig. 10. Precipitate size distributions $f(R^*)$ in the Fe-30%Cr-5%Al alloy irradiated to the irradiation dose $\phi = 6$ dpa in various regimes: (a) $T = 710$ K and $\mathcal{K} = 5 \times 10^{-7}$ dpa/s, (b) $T = 710$ K and $\mathcal{K} = 2 \times 10^{-6}$ dpa/s, (c) $T = 740$ K and $\mathcal{K} = 10^{-6}$ dpa/s. See further explanations in the text

and dashed curves in Figs. 7 and 8). Thus, a competition between the thermal and radiation-stimulated ballistic fluxes governs the dynamics of microstructural changes and statistical properties of precipitates. Namely, an increase of the irradiation temperature or a decrease of the dose rate enlarges the average size of precipitates and reduces their number.

Finally, let us analyze the influence of irradiation dose and irradiation conditions on the size distribution of the precipitates of the α'-phase. In Fig. 9, results obtained for the precipitate size distributions $f(R^*)$ in the Fe-30%Cr-5%Al alloy annealed and irradiated at $T = 710$ K and $\mathcal{K} = 10^{-6}$ dpa/s to various accumulated irradiation doses ϕ are presented. One can see that the distribution $f(R^*)$ remains universal as the accumulated dose increases. The obtained numerical data agree quite well with the Lifshitz–Slyozov–Wagner (LSW) distribution [51, 52] given by a solid curve. The difference is that the distributions obtained for the precipitates of the α'-phase via simulation are wider than the LSW ones and shifted toward larger R^*. This effect can be associated with the choice of the chromium concentration threshold x^c_{Cr}while determining the sizes of precipitates.

The spatial distribution of chromium concentration and the corresponding size distributions of precipitates under various irradiation conditions are illustrated in Fig. 10. The dashed curves correspond to the LSW distribution. As follows from the obtained results, at low defect formation rates (see Fig. 10,*a*), the numerically obtained distribution almost perfectly coincides with the LSW one. This is a result of the dominant thermal diffusion influence of microstructural changes in the material. An increase of the dose rate leads to the effects illustrated in Fig. 9: the growth of the number of precipitates whose sizes exceed the average value (Fig. 10,*b*). Here, as a result of the dominant ballistic irradiation, the precipitates become splintered (their average size becomes smaller, as is shown in Fig. 7). The irradiation temperature growth substantially accelerates the processes of microstructural transformations (see the above discussion of the results presented in Figs. 7 and 8). As a result, the number of precipitates is substantially reduced, and the obtained distribution differs from the LSW one (see Fig. 10,*c*). Thus, owing to the competition between the thermal diffusion and ballistic mixing, the irradiation conditions govern not only the dynamics of microstructural transformations but also the statistical properties of the precipitates of the α'-phase.

4. Conclusions

In this work, theoretical studies of the influence of irradiation temperature and damage rate on the microstructural evolution in Fe–Cr–Al alloys and the statistical properties of α'-phase precipitates under permanent neutron irradiation conditions.

In the framework of the linear stability analysis, the phase diagrams were plotted. They illustrate the system parameter intervals, where chromium precipitates are formed. It is shown that the addition of aluminum increases the critical temperature of precipitate stability and expands the chromium concentration interval, where phase separation processes are realized. It is found that the irradiation-induced ballistic mixing restricts the interval of precipitate stability parameters at low temperatures.

Using numerical simulation, the influence of irradiation conditions on the evolution of chromium precipitates available in the non-irradiated system and their statistical characteristics is analyzed. It is shown that the competition between the thermal diffusion and ballistic mixing governs the microstructural changes in the alloy under irradiation. It is found that an increase of the irradiation temperature leads to the same effects as a decrease of the defect formation rate; these are the acceleration of the phase decomposition dynamics, the larger average size of precipitates, and their smaller number. This effect can be explained as a result of the competition between ballistic mixing, which is responsible for the instability of the homogeneous configuration, and the thermodynamic force, which suppresses such instability.

The results obtained in this work concerning the influence of irradiation conditions and statistical characteristics of precipitates of the α'-phase are consistent with the results of previous studies [35, 36, 47].

The work was supported by the Ministry of Education and Science of Ukraine (grant No. 0124U000551).

1. J.F. Collins, F.C. Robertshaw. Advanced long-life reactor fuel cladding and structural materials development. *Sixth Annu. Rep. – High Temp. Mater. Programs Part A – GEMP* **475A**, 143 (1967).

2. P. Wang, Y. Qiao, W. Qi, S. Du, Z. Liu, F. Meng, X. Zhang, K. Wang, Q. Li, Z. Yao *et al.* Preparation and properties study of Cr on Fe–Cr–Al cladding materials. *Front. Mater.* **8**, 621086 (2021).
3. B.A. Pint, K.A. Terrani, M.P. Brady, T. Cheng, J.R. Keiser. High temperature oxidation of fuel cladding candidate materials in steam-hydrogen environments. *J. Nucl. Mater.* **440**, 420 (2013).
4. S.E. Sadique, A.H. Mollah, M.S. Islam, M.M. Ali, M.H.H. Megat, S. Basri. High-temperature oxidation behavior of iron–chromium–aluminum alloys. *Oxidat. Metals* **54**, 385 (2000).
5. E.A. Gulbransen, K.F. Andrew. Oxidation studies on the iron-chromium-aluminum heater alloys. *J. Electrochem. Soc.* **106**, 294 (1959).
6. K.A. Unocic, Y. Yamamoto, B.A. Pint. Effect of Al and Cr content on air and steam oxidation of Fe–Cr–Al alloys and commercial APMT alloy. *Oxidat. Metals* **87**, 431 (2017).
7. S.A. Briggs, P.D. Edmondson, K.C. Littrell, Y. Yamamoto, R.H. Howard, C.R. Daily *et al.* A combined APT and SANS investigation of α' phase precipitation in neutron-irradiated model Fe–Cr–Al alloys. *Acta Materialia* **129**, 217 (2017).
8. K.G. Field, S.A. Briggs. Radiation effects in Fe–Cr–Al alloys for nuclear power applications. In: *Reference Module3 in Materials Science and Materials Engineering* (Elsevier, 2020), p. 293.
9. S.S. Brenner, M.K. Miller, W.A. Soffa. Spinodal decomposition of iron-32 at.% chromium at 470 °C. *Scripta Metallurgica* **16**, 831 (1982).
10. S. Novy, P. Pareige, C. Pareige. Atomic scale analysis and phase separation understanding in a thermally aged Fe–20 at.% Cr alloy. *J. Nucl. Mater.* **384**, 96 (2009).
11. X. Xu, J. Odqvist, M.H. Colliander, M. Thuvander, A. Steuwer, J.E. Westraadt, S. King, P. Hedström. Structural characterization of phase separation in Fe-Cr: a current comparison of experimental methods. *Metallurg. Mater. Trans. A* **47**, 5942 (2016).
12. Z. Yang, Z. Wang, C. Xia, M. Ouyang, J. Peng, H. Zhang, X. Xiao. Aluminum suppression of α' precipitate in model Fe–Cr–Al alloys during long-term aging at 475 °C. *Mater. Sci. and Eng. A* **772**, 138714 (2020).
13. L. Malerba, A. Caro, J. Wallenius. Multiscale modelling of radiation damage and phase transformations: The challenge of FeCr alloys. *J. Nucl. Mater.* **382**, 112 (2008).
14. K. Chang, F. Meng, F. Ge, G. Zhao, S. Du, F. Huang. Theory-guided bottom-up design of the Fe–Cr–Al alloys as accident tolerant fuel cladding materials. *J. Nucl. Mater.* **516**, 63 (2019).
15. S. Chen, Y. Li, S. Shi, S. Jin *et al.* Quantitative phase-field simulation of composition partition and separation kinetics of nanoscale phase in Fe–Cr–Al alloy. *J. Nanomater.* **2019**, 6862390 (2019).
16. J. Lee, K. Park, K. Chang. Effect of al concentration on the microstructural evolution of Fe–Cr–Al systems: A phase-field approach. *Metals* **11**, 4 (2020).
17. L. Wu, J. Qin, V.O. Kharchenko, D.O. Kharchenko, O.B. Lysenko. Phase field modeling microstructural evolution of Fe–Cr–Al systems at thermal treatment. *Front. Energ. Res.* **11**, 1088742 (2023).
18. A.T. Dinsdale. SGTE data for pure elements. *Calphad* **15**, 317 (1991).
19. G. Martin. Phase stability under irradiation: Ballistic effects. *Phys. Rev. B* **30**, 1424 (1984).
20. V.G. Vaks, V.V. Kamyshenko. On the theory of open systems: Statistical thermodynamics and decomposition type phase transitions for the model of an alloy under irradiation. *Phys. Lett. A* **177**, 269 (1993).
21. S. Matsumura, Y. Tanaka, S. Müller, C. Abromeit. Formation of precipitates in an ordering alloy and their dissolution under irradiation. *J. Nucl. Mater.* **239**, 42 (1996).
22. C. Abromeit, H. Wollenberger, S. Matsumura. C. Kinoshita. Stability of ordered phases under irradiation. *J. Nucl. Mater.* **276**, 104 (2000).
23. R.A. Enrique, P. Bellon. Compositional patterning in systems driven by competing dynamics of different length scale. *Phys. Rev. Lett.* **84**, 2885 (2000).
24. R.A. Enrique, P. Bellon. Compositional patterning in immiscible alloys driven by irradiation. *Phys. Rev. B* **63**, 134111 (2001).
25. R.A. Enrique, K. Nordlund, R.S. Averback, P. Bellon. Simulations of dynamical stabilization of Ag–Cu nanocomposites by ion-beam processing. *J. Appl. Phys.* **93**, 2917 (2003).
26. R.A. Enrique, P. Bellon. Nonequilibrium fluctuations, effective temperature, and effective interactions driven by irradiation of alloys. *Phys. Rev. B* **70**, 224106 (2004).
27. D.O. Kharchenko, V.O. Kharchenko, I.O. Lysenko. Pattern selection processes and noise induced pattern-forming transitions in periodic systems with transient dynamics. *Open Phys,* **9**, 698 (2011).
28. D.O. Kharchenko, V.O. Kharchenko. Modeling phase decomposition and patterning in binary alloy systems subjected to neutron irradiation. *Radiat. Eff. Defect. Solids* **171**, 819 (2016).
29. D.O. Kharchenko, V.O. Kharchenko, Y.M. Ovcharenko, O.B. Lysenko, I.A. Shuda, L. Wu, R. Pan. Phase field modelling voids nucleation and growth in binary systems. *Condens. Matter Phys.* **21**, 1 (2018).
30. R. Averback, P. Bellon, S.J. Dillon. Phase evolution in driven alloys: An overview on compositional patterning. *J. Nucl. Mater.* **553**, 153015 (2021).
31. D.O. Kharchenko, A. Dvornichenko. Phase separation in binary systems with internal multiplicative noise. *Physica A* **387**, 5342 (2008).
32. S.I. Golubov, A. Barashev, R.E. Stoller. Radiation damage theory. In *Comprehensive Nuclear Materials. Edited by R.J.M. Konings* (Elsevier, 2012), Vol. 1, p. 357.
33. G.S. Was. *Fundamentals of Radiation Materials Science: Metals and Alloys* (Springer, 2017).

34. J.E. Hilliard. Spinodal decomposition. In: *Phase Transformations.* Edited by H.I. Aronson (American Society for Metals, 1970).
35. Z. Yan, S. Shi, Y. Li, J. Chen, S. Maqbool. Vacancy and interstitial atom evolution with the separation of the nanoscale phase in Fe–Cr alloys: Phase-field simulations. *Phys. Chem. Chem. Phys.* **22**, 3611 (2020).
36. L. Liang, Z.G. Mei, Y.S. Kim, M. Anitescu, A.M. Yacout. Three-dimensional phase-field simulations of intragranular gas bubble evolution in irradiated U-Mo fuel. *Comput. Mater. Sci.* **145**, 86 (2018).
37. G. Demange, L. Lunéville, V. Pontikis, D. Simeone. Prediction of irradiation induced microstructures using a multiscale method coupling atomistic and phase field modeling: Application to the AgCu model alloy. *J. Appl. Phys.* **121**, 125108 (2017).
38. C. Huang, M.O. de La Cruz, B.W. Swift. Phase separation of ternary mixtures: Symmetric polymer blends. *Macromolecules* **28**, 7996 (1995).
39. K. Wu,J. Morral, Y. Wang. A phase field study of microstructural changes due to the Kirkendall effect in two-phase diffusion couples. *Acta Materialia* **49**, 3401 (2001).
40. M. Norgett, M. Robinson, I.M. Torrens. A proposed method of calculating displacement dose rates. *Nucl. Eng. Design* **33**, 50 (1975).
41. J.H. Ke, E.R. Reese, E.A. Marquis, G.R. Odette, D. Morgan. Flux effects in precipitation under irradiation–Simulation of Fe–Cr alloys. *Acta Materialia* **164**, 586 (2019).
42. D. Terentyev, P. Olsson, T. Klaver, L. Malerba. On the migration and trapping of single self-interstitial atoms in dilute and concentrated Fe–Cr alloys: Atomistic study and comparison with resistivity recovery experiments. *Comput. Mater. Sci.* **43**, 1183 (2008).
43. S. Kim, W. Buyers. Vacancy formation energy in iron by positron annihilation. *J. Phys. F* **8**, L103 (1978).
44. C. Kittel, P. McEuen. *Introduction to Solid State Physics.* (John Wiley and Sons, 2018).
45. D. Terentyev, S. Hafez Haghighat,R. Schäublin. Strengthening due to Cr-rich precipitates in Fe–Cr alloys: effect of temperature and precipitate composition. *J. Appl. Phys.* **107**, 061806 (2010).
46. V. Ogorodnikov, A. Rakitskii, Y.I. Rogovoi. Calculation of the vacancy formation energy of metals. *Sov. Powder Metall. Met. Ceram.(Engl. Transl.);(United States)* **27**, 55 (1988)
47. K.G. Field, X. Hu, K.C. Littrell, Y. Yamamoto, L.L. Snead. Radiation tolerance of neutron-irradiated model Fe–Cr–Al alloys. *J. Nucl. Mater.* **465**, 746 (2015).
48. L.Q. Chen, J. Shen. Applications of semi-implicit Fourier-spectral method to phase field equations. *Comput. Phys. Commun.* **108**, 147 (1998).
49. C. Canuto, M. Hussaini, A. Quarteroni, A.Z. Thomas. *Spectral Methods In Fluid Dynamics* (Springer-Verlag, 1988).
50. S.B. Biner. *Programming Phase-Field Modeling* (Springer, 2017).
51. I.M. Lifshitz, V.V. Slyozov. *J. Phys. Chem. Solids* **19**, 35 (1961).
52. C. Wagner. Theorie der Alterung von Niederschlagen durch Umlosen (Ostwald-Reifung). *Z. Elektrochem* **65**, 581 (1961).

Received 29.05.24.
Translated from Ukrainian by O.I. Voitenko

В.О. Харченко, Д.О. Харченко,
А.В. Дворниченко, Б.О. Лисенко, С.В. Кохан

МОДЕЛЮВАННЯ ПРОЦЕСІВ МІКРОСТРУКТУРНИХ ПЕРЕТВОРЕНЬ У СПЛАВАХ Fe–Cr–Al ПРИ НЕЙТРОННОМУ ОПРОМІНЕННІ

Проведено теоретичні дослідження впливу умов опромінення на еволюцію мікроструктури сплавів Fe–Cr–Al та статистичні властивості преципітатів α'-фази. У рамках лінійного аналізу на стійкість встановлено фазові діаграми, що визначають область параметрів реалізації процесів випадіння преципітатів при термічному відпалі та опроміненні. У рамках числового моделювання досліджено вплив опромінення на кінетику преципітатів та зміну їх статистичних характеристик. Показано, що підвищення температури опромінення приводить до тих самих ефектів, що й зниження інтенсивності пошкодження унаслідок конкуренції між балістичним перемішуванням, відповідальним за нестабільність однорідної конфігурації, і термодинамічною силою, що пригнічує таку нестабільність.

Ключові слова: фазове розшарування, преципітати вторинних фаз, нейтронне опромінення, числове моделювання.